Seismic Analysis Of G+15 T-Shaped RC Building with Soil-Structure Interaction Using ETABS

Syed Khaleelullah Shah Quadri[1], Mohd Jamal Uddin[2]
[1]*Assistant Professor, Department of Civil Engineering, Nawab Shah Alam Khan College of Engineering and Technology, Hyderabad, India*
[2]*M.E Student, Department of Civil Engineering, Nawab Shah Alam Khan College of Engineering and Technology, Hyderabad, India*

Abstract*—Tall reinforced concrete buildings on soft or moderately stiff ground remain a persistent challenge in earthquake engineering, primarily because routine design practice continues to adopt the fixed-base assumption, which treats the supporting soil as perfectly rigid. Embedded in IS 1893 (Part 1): 2016, this assumption can meaningfully alter natural periods, redistribute seismic demand along the height, and shift the location of critical drift. This study evaluates soil-structure interaction (SSI) effects on a G+15 T-shaped RC framed building with a 300 mm core shear wall system modelled in ETABS under gravity, equivalent static seismic, and non-linear time-history loading. Two models are compared: a fully fixed-base model and an SSI model employing discrete Winkler point springs ($K_x = K_y = 10{,}000$ kN/m lateral; $K_{45} = 40{,}000$ kN/m vertical). The fundamental period elongates from 2.308 s (fixed) to 3.364 s (SSI), an increase of 45.8%. Under EQX equivalent static loading, SSI amplifies roof displacement nearly 2.83 times (47 mm → 132.9 mm), whereas EQY amplification is marginal owing to the inherent plan stiffness of the T-shape. SSI shifts the critical inter-storey drift zone from mid-height (Storeys 3–5) to the Base–Storey 2 interface, where drifts of 0.004616 (EQX) and 0.004411 (EQY) marginally exceed the IS 1893 limit of 0.004. Non-linear time-history analysis using five PEER NGA-West2 records confirms satisfactory performance, with all individual peak drifts below 0.000384—less than 10% of the permissible limit. P-M-M interaction ratios for all columns remain within acceptable bounds. The results demonstrate that a fixed-base model systematically underestimates displacement demand and misidentifies the critical drift zone, confirming that explicit SSI modelling is essential for a realistic seismic performance assessment of tall RC buildings on deformable soils.

***Index Terms*—Soil-structure interaction; T-shaped RC building; ETABS; period elongation; inter-storey drift; non-linear time-history analysis; IS 1893: 2016; Winkler spring; seismic performance.**

I. INTRODUCTION

The seismic design of high-rise reinforced concrete (RC) moment-resisting frame (MRF) buildings is an increasingly critical challenge in earthquake engineering, particularly in urbanising seismic zones where vertical development on challenging ground conditions is prevalent. Among the most consequential yet frequently neglected factors are soil-structure interaction (SSI): the coupled dynamic response of a structure and its supporting soil under seismic loading. Conventional seismic design, codified in IS 1893 (Part 1): 2016 and most international standards, assumes a rigidly restrained base (fixed-base assumption). While computationally convenient, this idealisation can introduce significant inaccuracies in predicting natural periods, mode shapes, base shear, inter-storey drift ratios (ISDRs), and roof displacements—with tangible consequences for structural safety, particularly for tall buildings on soft soil.

Soft soils with shear-wave velocities $V_s \leq 180$ m/s constitute a significant proportion of the urban sub-surface profile in Indian cities such as Bengaluru, Chennai, Mumbai, and Kolkata. Landmark seismic events—the 1985 Michõacán earthquake (M^L 8.0), the 1995 Kobe earthquake (M^L 6.9), and the 2011 Christchurch earthquakes—confirmed that ignoring SSI can lead to systematic under-estimation of drift demands and incorrect identification of the critical damage zone.

IS 1893 (Part 1): 2016 acknowledges SSI in Clause 6.15 but provides no quantitative procedures for routine implementation. The present study addresses this gap through a comprehensive numerical investigation of a G+15 T-shaped RC building with a 300 mm shear wall core in ETABS, comparing fixed-base and SSI (Winkler spring) responses under equivalent static and non-linear time-history seismic loading.

A. Objectives

1) Develop a 3-D finite element model of the G+15 T-shaped RC building in ETABS with both fixed-base and SSI configurations, designed to IS 1893: 2016 and IS 456: 2000.
2) Perform modal analysis (12 modes) and compare natural periods; conduct equivalent static and NLTHA using five PEER NGA-West2 records.
3) Examine directional sensitivity of SSI amplification under X- and Y-direction loading and identify the shift in critical drift location due to foundation flexibility.
4) Verify column adequacy through P-M-M interaction checks and derive practical design guidance on consequences of ignoring soil flexibility.

II. LITERATURE REVIEW

A. Theoretical Foundations

Veletsos and Meek (1974) introduced the concept of elongated period and effective damping for inertial SSI, demonstrating that the two governing dimensionless parameters are the structure-to-soil stiffness ratio h/V_sT and the mass ratio α_m. Veletsos and Verbic (1973) derived frequency-dependent impedance functions for circular foundations; Gazetas (1991) extended these to arbitrarily shaped foundations on layered half-spaces. Wolf (1985, 1994) developed cone models as computationally efficient alternatives. Jennings and Bielak (1973) established formal equations of motion for the coupled soil-structure system, underpinning both substructure and direct analysis approaches.

B. SSI Effects on RC Buildings

Oz et al. (2020) showed that SSI significantly increases lateral displacements and reduces base shear in low- and mid-rise RC frames on soft soils, making the fixed-base assumption unconservative for deformation-sensitive damage states. Wani et al. (2022) reported storey drift increases in high-rise RC structures with raft foundations and cautioned that the IS 1893 empirical period formula underestimates the SSI-elongated period. Bapir et al. (2024) confirmed that SSI alters modal properties and increases vulnerability in mid- to high-rise buildings.

For high-rise structures, Mata (2023) found that SSI increases collapse probability in fragility curves. Zhang and Far (2024) demonstrated that SSI effects are strongly dependent on soil type, foundation system, and height. Hamida et al. (2021) showed that nonlinear soil behaviour reduces collapse margin ratios relative to fixed-base conditions for 20-storey steel MRF frames. Kalapodis et al. (2025) found fundamental period elongation up to 15% for soft soil conditions, leading to overestimation of base shear in fixed-base models.

C. Research Gap

Most parametric SSI investigations focus on low- to mid-rise structures (4–12 storeys) or steel frames. Comprehensive 3-D nonlinear analyses of RC MRF buildings at exactly G+15 storeys on Indian-code-compatible soil profiles are limited. IS 1893 provides no quantitative SSI implementation procedures, unlike ASCE/SEI 7-22 and Eurocode 8. The present study is designed to address these gaps.

III. STRUCTURAL MODEL AND METHODOLOGY

A. Building Configuration

The building is a G+15 RC framed structure with a T-shaped plan, bay widths of 8.0 m (X) and 7.0 m (Y), and a uniform storey height of 3.0 m. The lateral load-resisting system combines RC moment frames with 300 mm thick shear walls positioned along the core and peripheral bays. Column sections are 600 mm × 600 mm from ground level to Storey 8, tapering to 530 mm × 530 mm above, reflecting the reduction in axial demand with height. Concrete grade is M40 with HYSD Fe-500 reinforcement. Key structural parameters are summarised in Table I.

TABLE I. STRUCTURAL CONFIGURATION AND MATERIAL PROPERTIES

Parameter	Value / Description
Building Type	Residential / Commercial (G+15)
Plan Shape	T-shaped
Number of Storeys	G+15 (Total height = 48 m)
Storey Height	3.0 m (all floors)
Bay Width X / Y	8.0 m / 7.0 m
Concrete Grade	M40
Steel Grade	HYSD Fe-500 (500 N/mm²)
Column G+0 to G+8	600 mm × 600 mm
Column G+9 to G+15	530 mm × 530 mm
Beam Depth	450 mm (uniform all floors)
Shear Wall Thickness	300 mm
Live Load on Slab	3.0 kN/m²
Superimposed DL on Beam	3.65 kN/m²
Seismic Zone	Zone II (IS 1893: 2016)
Foundation Model	Point spring supports (SSI model)

B. T-Shaped Floor Plan

The T-shaped plan introduces a plan irregularity resulting in an eccentric distribution of mass and stiffness relative to the geometric centre. This eccentricity has direct implications on the torsional response under seismic excitation. The floor plan is shown in Fig. 1.

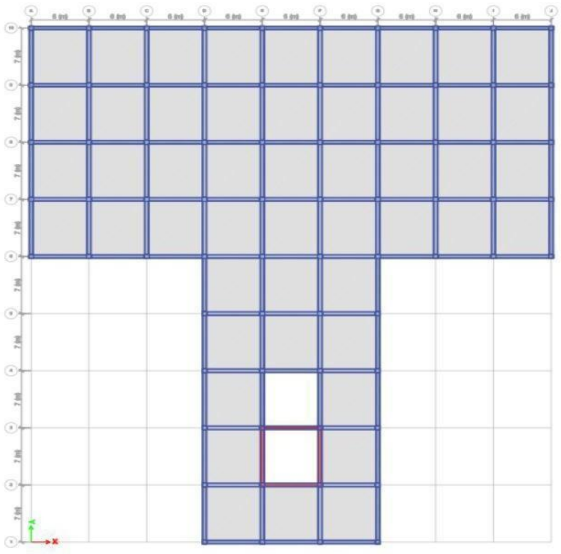

Fig. 1: T-Shaped Floor Plan of the G+15 Building

C. Three-Dimensional Structural Model

A three-dimensional wireframe model was developed in ETABS, incorporating all beams, columns, slabs, and shear walls. Shear wall elements are modelled as shell elements; beam and column members as frame elements with appropriate end offsets. The 3D models are presented in Figs. 2 and 3.

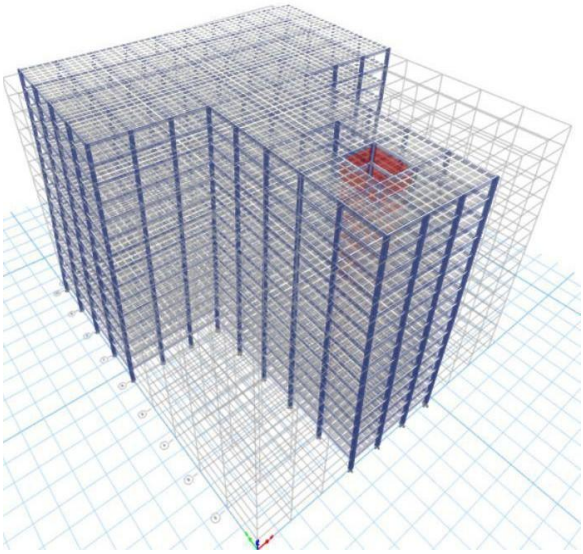

Fig. 2: 3D Mesh Model of the T-Shaped G+15 Building

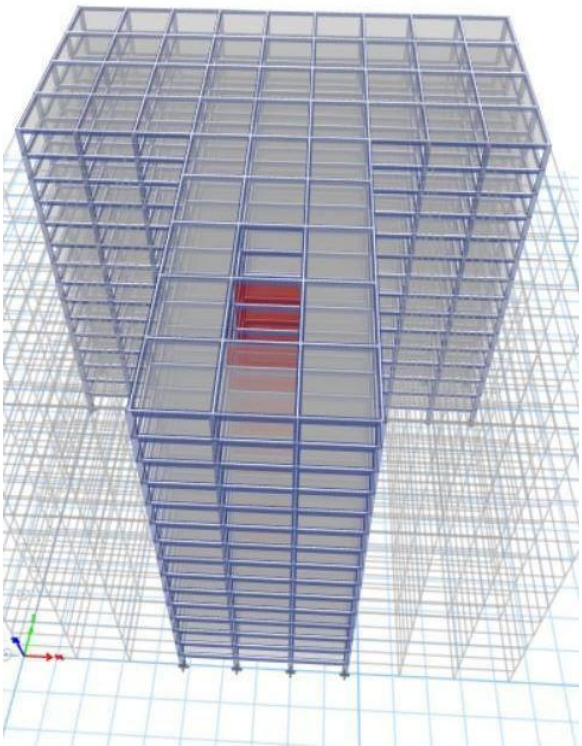

Fig. 3: T-Shaped Structural Configuration — 3D View

D. Shear Wall Layout and Spring Foundation

The 300 mm thick shear walls are positioned along the core region and peripheral bays, designed to resist lateral forces in both X and Y directions while controlling torsional effects. Point spring supports are assigned at each column base node to model SSI; the spring stiffness values are derived from the modulus of subgrade reaction of the supporting soil (Table II). Figs. 4 and 5 illustrate the shear wall arrangement and the spring support configuration.

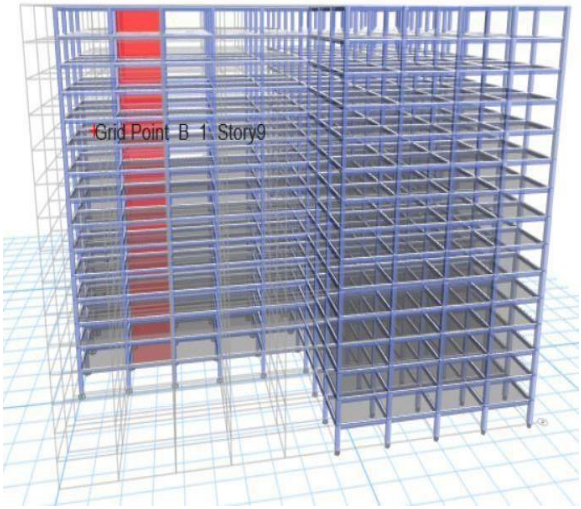

Fig. 4: 3D Plan View Showing Shear Wall (Red) Positions — Storey 9

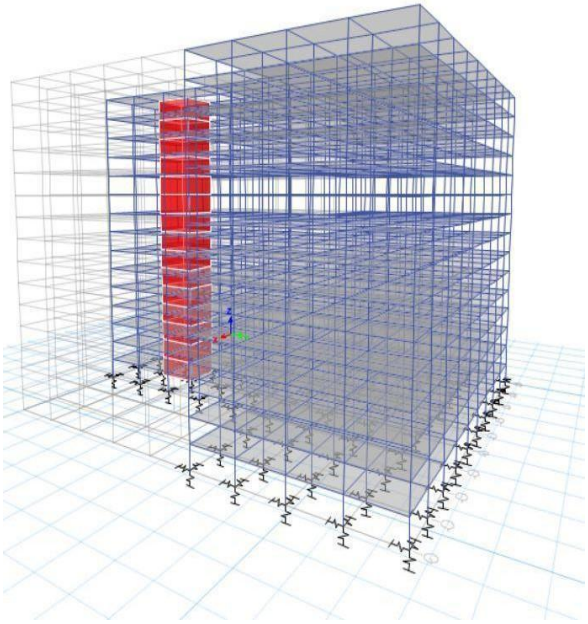

Fig. 5: Spring Support Model Showing Soil-Structure Interaction at Foundation Level

TABLE II. POINT SPRING STIFFNESS PROPERTIES — SSI MODEL

Direction	Stiffness (kN/m)	Unit	Interpretation
Translation X	10,000	kN/m	Lateral soil resistance X-direction
Translation Y	10,000	kN/m	Lateral soil resistance Y-direction
Translation Z	40,000	kN/m	Vertical / bearing resistance
Rotation (all axes)	0	kN-m/rad	No rotational springs assigned

E. Ground Motions for NLTHA

Non-linear time-history analysis was performed using five real accelerograms from the PEER NGA-West2 database, drawn from the 1979 Coyote Lake (M^L 5.74) and 1989 Loma Prieta (M^L 6.93) earthquakes, spanning PGAs of 0.35–0.55 g (Table III).

TABLE III. PEER NGA-WEST2 GROUND MOTION RECORDS USED IN NLTHA

RSN	File Name	Earthquake	Year	Mw	PGA (g)
147	RSN147_COYOTELK_G02140	Coyote Lake, CA	1979	5.74	0.35
149	RSN149_COYOTELK_G04-UP	Coyote Lake, CA	1979	5.74	0.55
149	RSN149_COYOTELK_G04270	Coyote Lake, CA	1979	5.74	0.40
149	RSN149_COYOTELK_G04360	Coyote Lake, CA	1979	5.74	0.40
764	RSN764_LOMAP_GOF160	Loma Prieta, CA	1989	6.93	0.35

IV. RESULTS AND DISCUSSION

A. Modal Analysis — Fixed-Base Model

Modal analysis was performed over 12 modes to achieve ≥90% cumulative mass participation in both principal directions, as required by IS 1893: 2016. The fundamental mode has a period of 2.308 s and a frequency of 0.433 cyc/s, reflecting the flexible lateral response of the 15-storey building. Results are presented in Table IV.

TABLE IV. MODAL ANALYSIS RESULTS — FIXED-BASE MODEL

Mode	Period (s)	Freq. (cyc/s)	Circ. Freq. (rad/s)	Eigenvalue (rad²/s²)
1	2.308	0.433	2.7219	7.4086
2	1.701	0.588	3.6934	13.6414
3	1.285	0.778	4.8897	23.9096
4	0.777	1.287	8.0854	65.3735
5	0.468	2.135	13.4139	179.9336
6	0.453	2.209	13.8793	192.6352
7	0.358	2.797	17.5721	308.7804
8	0.316	3.165	19.8860	395.4513
9	0.249	4.018	25.2461	637.3643
10	0.236	4.230	26.5775	706.3653
11	0.231	4.333	27.2268	741.2993
12	0.195	5.141	32.2997	1043.2725

B. Modal Analysis — SSI Model

When fixed-base restraints are replaced by discrete translational springs, the fundamental period elongates from 2.308 s to 3.364 s—an increase of approximately 45.8%. The second and third modes also exhibit pronounced elongation; from Mode 4 onward the SSI periods converge progressively towards the fixed-base values, with Mode 12 showing only a 9.7% difference (Table V).

TABLE V. MODAL ANALYSIS RESULTS — SSI (POINT SPRING) MODEL

Mode	Period (s)	Freq. (cyc/s)	Circ. Freq. (rad/s)	Eigenvalue (rad²/s²)
1	3.364	0.297	1.8678	3.4888
2	3.274	0.305	1.9192	3.6833
3	2.798	0.357	2.2459	5.0441
4	0.981	1.019	6.4048	41.0220
5	0.866	1.155	7.2552	52.6383
6	0.758	1.319	8.2862	68.6606
7	0.528	1.895	11.9084	141.8109
8	0.361	2.772	17.4175	303.3686
9	0.349	2.867	18.0147	324.5282
10	0.287	3.484	21.8882	479.0937
11	0.264	3.792	23.8289	567.8155
12	0.214	4.675	29.3713	862.6733

TABLE VI. NATURAL PERIOD COMPARISON — FIXED-BASE vs. SSI MODEL

Mode	Description	Fixed-Base (s)	SSI (s)	Elongation (%)
1	Translational X	2.308	3.364	+45.8
2	Translational Y	1.701	3.274	+92.5
3	Torsional	1.285	2.798	+117.7
4	—	0.777	0.981	+26.3
12	—	0.195	0.214	+9.7

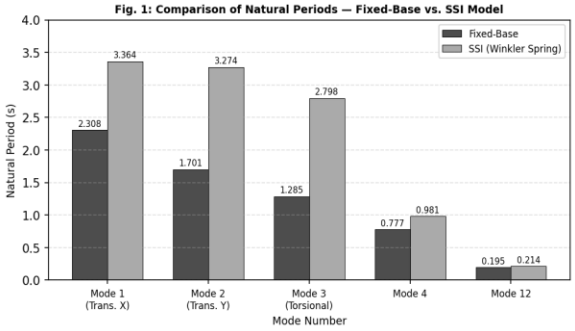

Fig. 6: Bar Chart — Natural Period Comparison, Fixed-Base vs. SSI Model

C. Gravity Load Analysis — Fixed-Base Model

Under gravity loading, the fixed-base model produces negligible lateral displacements (of the order of 10^{-3} mm). The maximum inter-storey drift of 0.001964 is recorded between Storeys 3 and 5, within the IS 1893 serviceability limit of 0.002. The drift profile is shown in Fig. 7; the overturning moment diagram in Fig. 8.

TABLE VII. MAXIMUM STOREY DRIFTS UNDER GRAVITY LOADS (FIXED-BASE)

Storey	Max Drift (Dimensionless)	Allowable (IS 1893)	Status
Base	0.000000	0.002	OK
Story 2	0.000180	0.002	OK
Story 5	0.001200	0.002	OK
Story 8	0.001820	0.002	OK
Story 11	0.001940	0.002	OK
Story 15 (max)	0.001964	0.002	OK — within limit

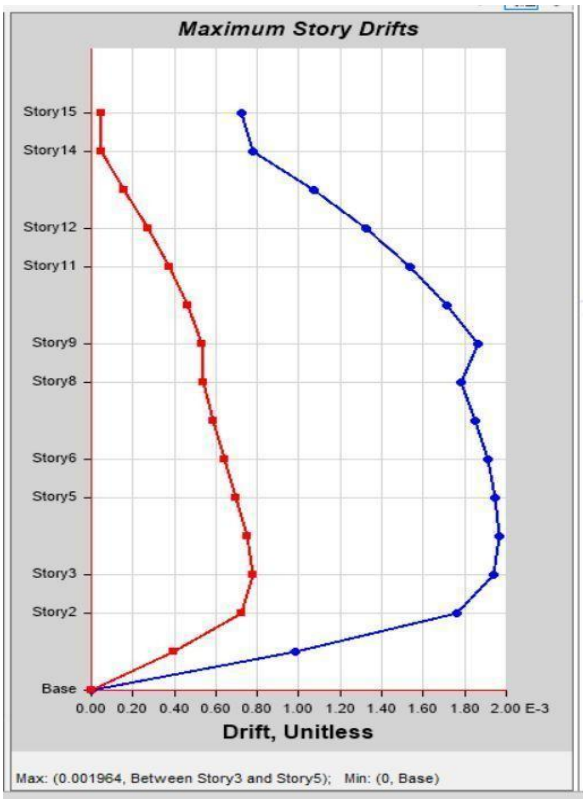

Fig. 7: Maximum Storey Drift Profile under Gravity Loads — Fixed-Base Model

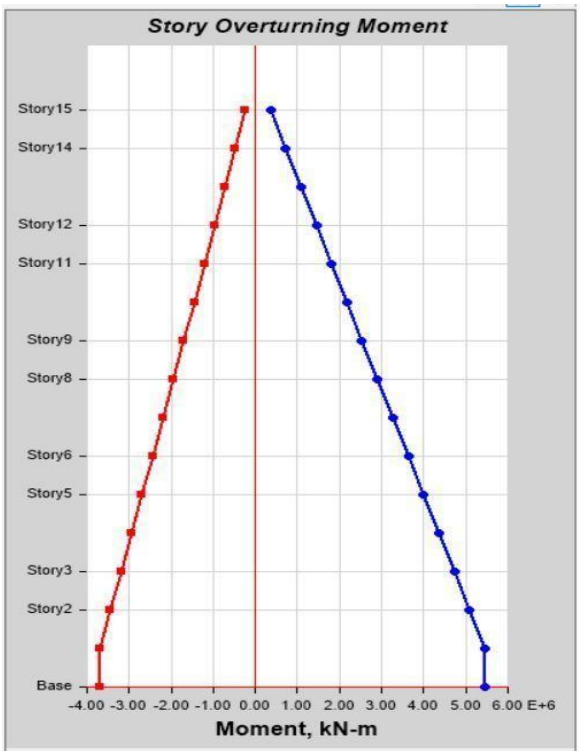

Fig. 8: Storey Overturning Moment under Gravity Loads — Fixed-Base Model

D. Seismic Analysis: Fixed-Base Model (EQX)

Under EQX equivalent static loading the maximum roof displacement reaches approximately 47 mm, following a near-linear, flexure-dominated profile consistent with shear wall behaviour (Fig. 9). The displacement profile confirms the shear wall system is mobilising the intended flexural mechanism with no evidence of soft-storey concentration.

TABLE VIII. MAXIMUM STOREY DISPLACEMENT UNDER EQX (FIXED-BASE)

Storey	Min Displacement (mm)	Max Displacement (mm)	Trend
Base	0.00	0.00	Zero — fixed restraint
Story 2	0.5	1.5	Linear commencement
Story 5	3.0	8.0	Continuing increase
Story 8	5.0	16.0	Mid-height zone
Story 12	10.0	30.0	Accelerating
Story 15 (max)	13.5	47.0	Peak roof displacement

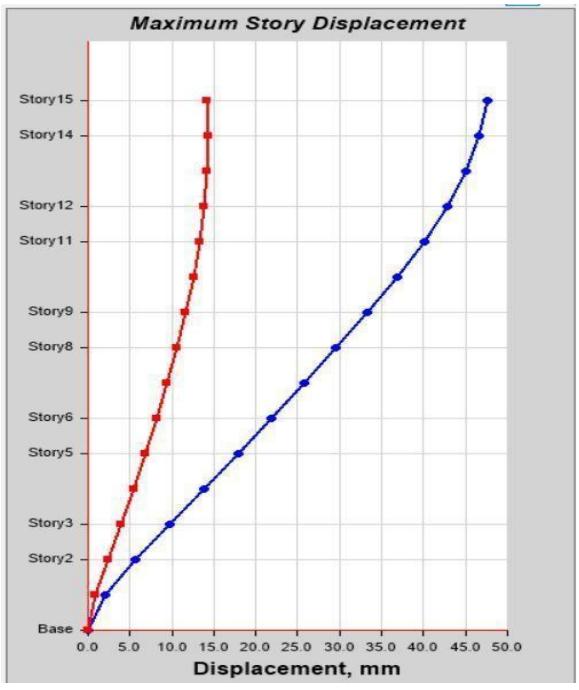

Fig. 9: Maximum Storey Displacement Profile under EQX — Fixed-Base Model

E. Seismic Analysis: Fixed-Base Model (EQY)

The maximum storey drift under EQY of 0.001326 is recorded at Storey 15, with a secondary peak of 1.050 × 10^{-3} at Storey 9. All values remain below the IS 1893: 2016 permissible limit of 0.002 (Fig. 10). Table IX presents the drift profile.

TABLE IX. MAXIMUM STOREY DRIFTS UNDER EQY LOADING (FIXED-BASE)

Storey	Max Drift Y (×10^{-3})	Critical Zone	Allowable	Remarks
Base	0.000	No	0.002	Zero drift at base
Story 6	0.600	No	0.002	Moderate
Story 9	1.050	Yes	0.002	Secondary peak zone
Story 11	0.900	Yes	0.002	Elevated drift
Story 15 (max)	1.326	Yes	0.002	Maximum recorded drift

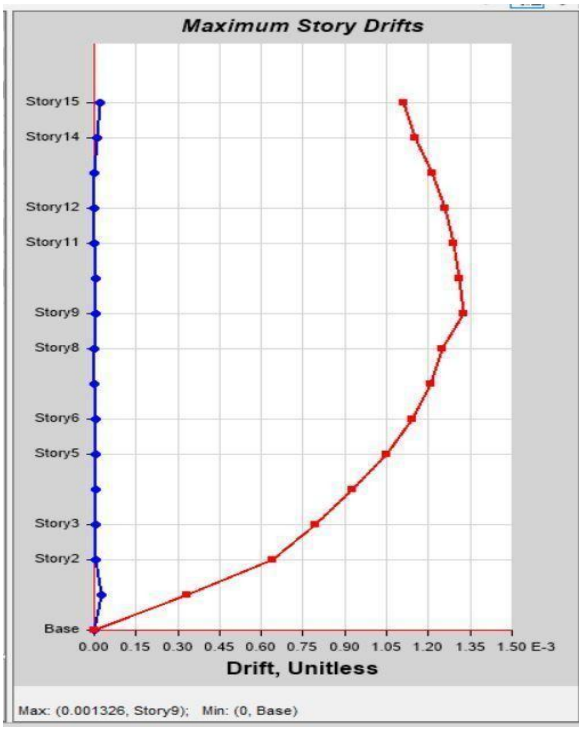

Fig. 10: Maximum Storey Drift Profile under EQY — Fixed-Base Model

F. Comparative Assessment: Gravity vs. Seismic (Fixed-Base)

Under gravity loads, lateral displacements are of the order of 10^{-3} mm throughout the height of the building; under EQX seismic loading, displacements increase continuously with height, reaching 47 mm at the roof (Fig. 11). The near-linear EQX profile confirms a flexure-dominated shear wall response.

G. SSI Analysis — Point Spring Stiffness Assignment

Fig. 12 shows the point spring stiffness assignment in ETABS with translational springs in all three global directions. The vertical spring (40,000 kN/m) is set to four times the lateral springs (10,000 kN/m each), reflecting the higher bearing resistance of soils to vertical compression versus horizontal shear.

Fig. 11: Point Spring Stiffness Assignment in ETABS (Translational Springs in Global Directions)

H. SSI Analysis Gravity Load Response

The SSI model produces measurable gravity displacements of up to 6.0 mm at roof level due to spring settlement (Fig. 13). Inter-storey drifts under gravity with SSI are of the order of 10^{-6} (Fig. 14)—well within permissible limits, confirming that SSI introduces negligible drift demand under gravity loading alone.

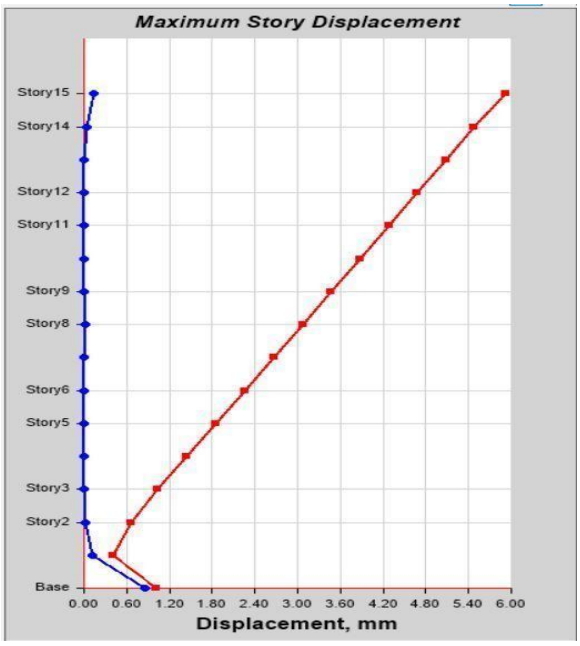

Fig. 12: Maximum Storey Displacement under Gravity Loads — SSI Model

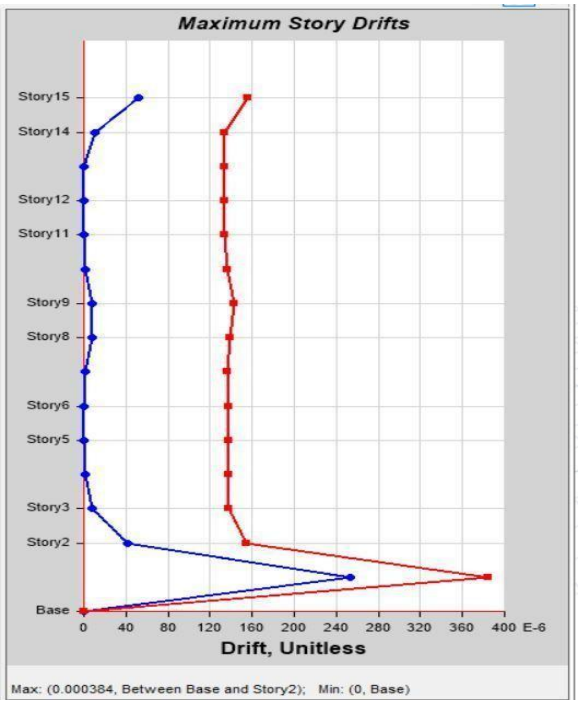

Fig. 13: Maximum Storey Drifts under Gravity Loads — SSI Model

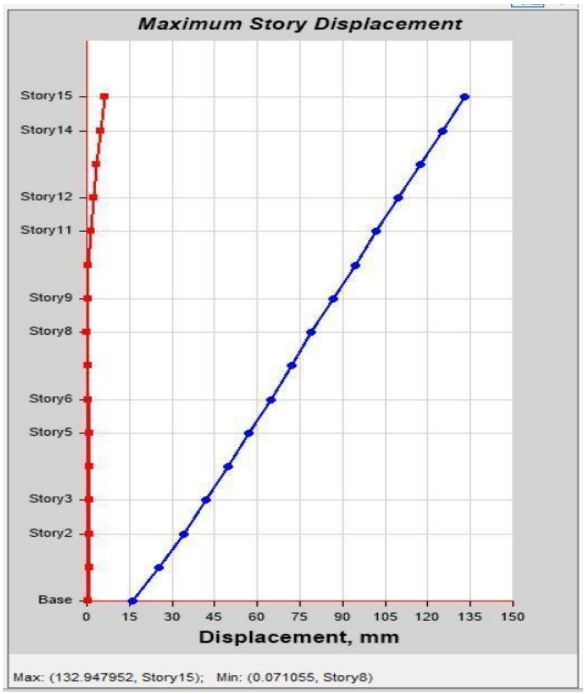

Fig. 14: Maximum Storey Displacement under EQX Loading — SSI Model

I. SSI Analysis — Seismic Response (EQX)

The SSI model registers a non-zero-base displacement of approximately 15 mm under EQX, arising from spring translation. This base displacement stacks onto the cantilever drift of the superstructure, amplifying the roof displacement from 47 mm (fixed-base) to 132.9 mm under SSI—an amplification factor of 2.83 (Fig. 15). The inter-storey drift reaches a maximum of 0.004616 at the Base–Story 2 interface, marginally exceeding the IS 1893 limit of 0.004 by 15.4% (Fig. 16 and Table X).

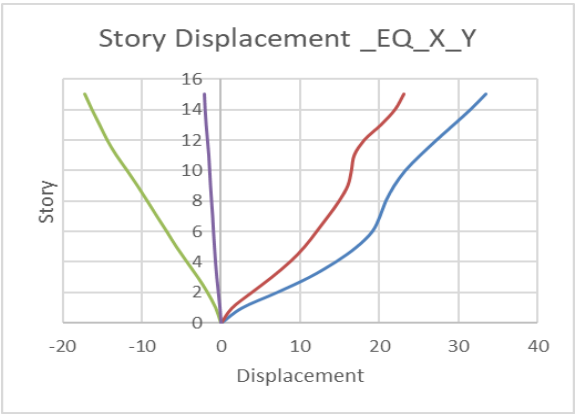

Fig. 15: Maximum Inter-Storey Drift under EQX Loading — SSI Model

TABLE X. STOREY DISPLACEMENT COMPARISON UNDER EQX — FIXED-BASE vs. SSI

Storey	Fixed-Base (mm)	SSI Max (mm)	SSI Min (mm)	Remarks
Base	0.00	15.0	0.07	Spring flexibility
Story 5	8.0	45.0	—	Linear increase
Story 8	16.0	70.0	0.071	Mid-height zone
Story 11	24.0	100.0	—	Upper zone
Story 15 (max)	47.0	132.9	—	SSI: 2.83× fixed-base

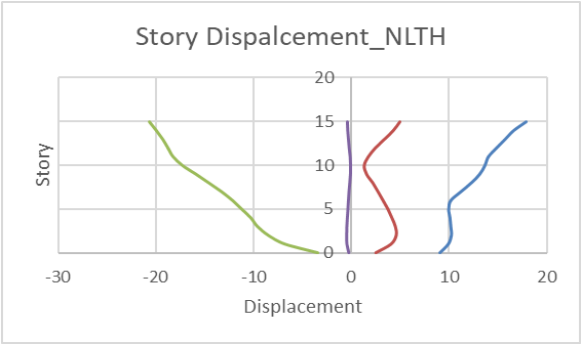

Fig. 16: Storey Displacement Profile underNLTHA Fixed-Base vs. SSI (Graphical Comparison)

J. SSI Analysis: Seismic Response (EQY)

Under EQY with SSI, the maximum roof displacement is 118.594 mm—comparable to the fixed-base result of ~118 mm (amplification ratio ≈1.0). The T-shaped plan is inherently stiffer in the Y-direction, moderating SSI amplification considerably. The base-zone drift of 0.004411 marginally exceeds the IS 1893 limit by 10.3% (Figs. 18 and 19).

TABLE XI. STOREY DISPLACEMENT COMPARISON UNDER EQY: FIXED-BASE vs. SSI

Storey	Fixed-Base (mm)	SSI Max (mm)	Amplification	Remarks
Base	0	12–15	—	Spring flexibility
Story 5	25	48	1.9	Moderate amplification
Story 8	40	72	1.8	Consistent increase
Story 11	80	96	1.2	Reducing ratio
Story 15 (max)	118.6	118.6	1.0	Marginal amplification at roof

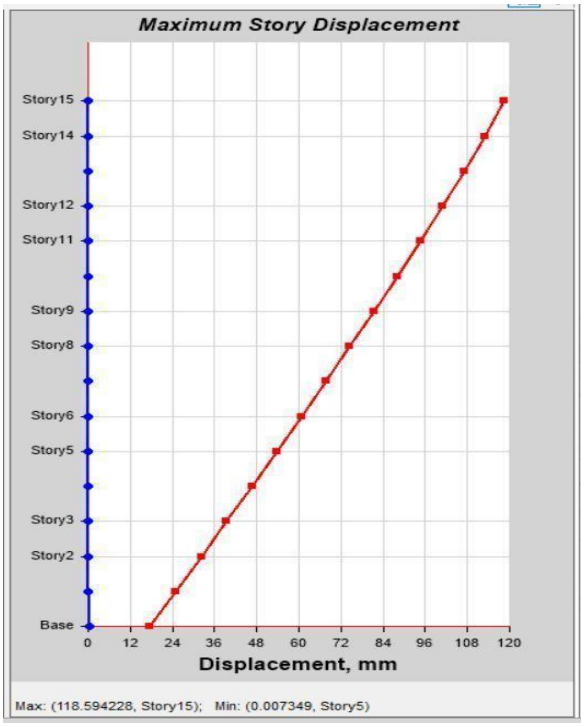

Fig. 17: Maximum Storey Displacement under EQY Loading — SSI Model

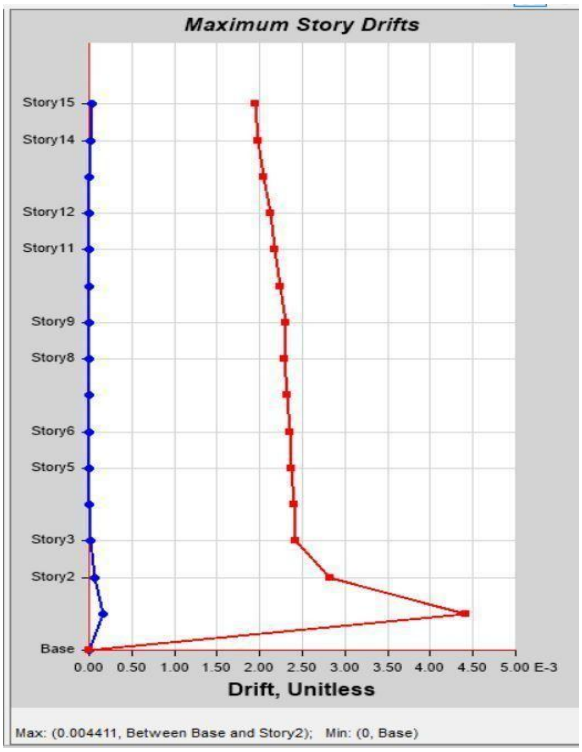

Fig. 18: Maximum Storey Drifts under EQY Loading — SSI Model

K. Non-Linear Time History Analysis (NLTHA)

NLTHA was performed using five PEER NGA-West2 records with SSI spring supports. Across all ground motions, all individual drift values remain substantially below the IS 1893 limit of 0.004. The maximum recorded drift of 0.000384 (GM-6, Base–Story 2) represents only 9.6% of the permissible limit, demonstrating that the equivalent static method is considerably conservative. Individual NLTHA drift profiles are shown in Figs. 20–25; results are summarised in Table XII.

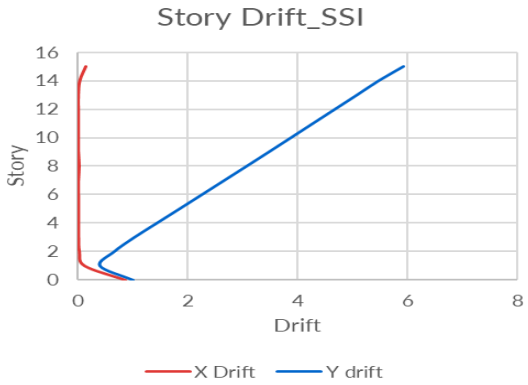

Fig. 19: Summary NLTHA Maximum Inter-Storey Drifts vs. IS 1893 Limit (SSI Model)

TABLE XII. NLTHA INTER-STOREY DRIFT RESULTS — ALL GROUND MOTIONS (SSI MODEL)

GM	Record	Max Drift	Location	vs. Limit (0.004)
1	RSN147 — G02140	0.000190	Base–Story 2	4.75% of limit
2	RSN149 — G04-UP	0.000149	Base–Story 2	3.73% of limit
3	RSN149 — G04270	0.000094	Story 14	2.35% of limit
4	RSN149 — G04360	0.000286	Base–Story 2	7.15% of limit
5	RSN764 — GOF160	0.000154	Story 11	3.85% of limit
6	Additional Record	0.000384	Base–Story 2	9.60% of limit (maximum)

L. Column P-M-M Interaction Check

P-M-M interaction ratios for all column sections under all governing load combinations (IS 456: 2000) remain below 1.0, with values ranging from 0.8% to 6.0%. This confirms structural adequacy with substantial reserve capacity margin; no section revision is required.

M. Consolidated Comparison: Fixed-Base vs. SSI

Table XIII consolidates the key response parameters from both models.

TABLE XIII. CONSOLIDATED COMPARISON — FIXED-BASE vs. SSI MODEL

Response Parameter	Fixed-Base	SSI	Observation
Fundamental period	2.308 s	3.364 s	+45.8% elongation
Gravity max. displacement	35×10^{-3} mm	6.0 mm	SSI 170× larger (absolute)
Gravity max. drift	0.001964 (Story 3–5)	0.000190 (Base–S2)	SSI drift at micro level
EQX roof displacement	47 mm	132.9 mm	SSI 2.83× amplification
EQY roof displacement	118 mm	118.6 mm	Marginal (≈1.0×)
EQX max drift	Within 0.004	0.004616 (Base–S2)	Exceeds by 15.4%
EQY max drift	Within 0.004	0.004411 (Base–S2)	Exceeds by 10.3%
NLTHA max drift (any GM)	—	0.000384	9.6% of limit
Critical drift zone	Story 3–5	Base–Story 2	SSI shifts zone to base
P-M-M ratio	<1.0	0.8%–6.0%	All within limit

V. PERIOD ELONGATION CALCULATION

The percentage elongation of the fundamental natural period due to SSI is:

Elongation (%) = (TSSI − TFixed) / TFixed × 100= (3.364 − 2.308) / 2.308 × 100 = 1.056 / 2.308 × 100 = 45.76%

This elongation indicates that the structure becomes substantially more flexible when soil compliance is accounted for. A shift in fundamental period from 2.308 s to 3.364 s moves the spectral demand from the acceleration-controlled plateau of the IS 1893: 2016 design spectrum into the displacement-sensitive region, reducing inertial force demand while significantly increasing lateral displacement demand. This confirms that the fixed-base assumption underestimates deformation demand and that explicit SSI modelling is necessary for a realistic performance assessment.

VI. CONCLUSIONS

The following conclusions are drawn from the seismic analysis of the G+15 T-shaped RC building:

1) The G+15 T-shaped RC building with a 300 mm shear wall system satisfies all serviceability and strength requirements of IS 456: 2000 and IS 1893: 2016 under both gravity and seismic loading.

2) SSI elongates the fundamental natural period from 2.308 s to 3.364 s (+45.8%), shifting spectral demand from the acceleration plateau to the displacement-sensitive branch. Higher modes elongate even more (Modes 2 and 3: +92.5% and +117.7% respectively).
3) Under EQX seismic loading, SSI amplifies roof displacement from 47 mm to 132.9 mm (factor of 2.83) driven predominantly by base translation of the spring-supported foundation. Under EQY loading, amplification is marginal (≈1.0×) owing to the higher plan stiffness of the T-shape in that direction.
4) SSI shifts the critical inter-storey drift zone from mid-height (Storeys 3–5) in the fixed-base model to the Base–Story 2 interface. Equivalent static SSI drifts of 0.004616 (EQX) and 0.004411 (EQY) marginally exceed the IS 1893 limit of 0.004 by 15.4% and 10.3%, demanding enhanced reinforcement detailing at the base zone.
5) NLTHA under five real ground motions confirms satisfactory dynamic performance with SSI; all individual drift values remain well within the permissible limit (maximum 0.000384, or 9.6% of the limit), demonstrating that the equivalent static method is considerably conservative.
6) P-M-M interaction ratios for all column sections remain between 0.8% and 6.0%, confirming structural adequacy under all governing load combinations without section revision.
7) A fixed-base analysis systematically underestimates displacement demand and misidentifies the critical drift zone. Explicit SSI modelling is therefore essential for a realistic seismic performance assessment of tall RC buildings on deformable soils, and provides strong grounds for updating IS 1893 to include quantitative SSI implementation procedures analogous to ASCE/SEI 7-22 and Eurocode 8.

ACKNOWLEDGMENT

The authors acknowledge the computational resources provided by the Department of Civil Engineering,

REFERENCES

[1] B. Bapir, L. Abrahamczyk, T. Wichtmann, and L. F. Prada-Sarmiento, “Soil-structure interaction: A state-of-the-art review,” *Frontiers in Built Environment*, vol. 9, pp. 1–25, 2024.
[2] P. Debnath, T. Das, and D. Choudhury, “Influence of soil-structure interaction and ground motion parameters on the seismic vulnerability of RC buildings,” Scientific Reports, 2026.
[3] D. Forcellini, “Fragility curves for RC buildings with SSI for tall building assessment,” Bulletin of Earthquake Engineering, vol. 20, no. 12, pp. 6765–6791, 2022.
[4] Z. Hamida, J. D. Nzabonimpa, and W. K. Hong, “Effects of SSI on the seismic collapse capacity of steel moment-resisting frames,” J. Building Engineering, vol. 44, p. 103036, 2021.
[5] P. Jagan and J. A. Visuvasam, “Assessment of nonlinear SSI effects on RC structures with floating columns,” Geomatics, Natural Hazards and Risk, vol. 15, no. 1, p. 2401997, 2024.
[6] N. A. Kalapodis, G. A. Papagiannopoulos, and D. E. Beskos, “Quantifying the impact of SSI on performance-based seismic design of steel MRF buildings,” Buildings, vol. 15, no. 20, p. 3741, 2025.
[7] M. S. Kirçil and H. Ethemoglu, “Effect of SSI on the damage probability of multistory RC frame buildings,” Buildings, vol. 15, no. 4, p. 624, 2025.
[8] R. Mata, “Seismic SSI effects on RC moment frame buildings designed to modern codes,” J. Earthquake Engineering, vol. 27, no. 10, pp. 2841–2865, 2023.
[9] I. A. Najar et al., “Advancing soil-structure interaction (SSI): A comprehensive review,” J. Infrastructure Preservation and Resilience, vol. 6, Art. no. 5, 2025.
[10] P. Oggu, K. Gopikrishna, and S. Nagarajaiah, “Assessment of SSI effects on fragility and ductility demands of RC MRFs,” J. Earthquake Engineering, vol. 29, no. 2, pp. 345–371, 2025.
[11] I. Oz, S. M. Senel, M. Palanci, and A. Kalkan, “Effect of SSI on the seismic response of existing low and mid-rise RC buildings,” Applied Sciences, vol. 10, no. 23, p. 8357, 2020.
[12] C. Petridis, “Fragility curve modifiers for RC dual buildings accounting for SSI effects,” Earthquake Engineering and Structural Dynamics, vol. 51, no. 9, pp. 2055–2076, 2022.
[13] D. Pitilakis, “Soil-structure interaction and site amplification effects on fragility curves for RC moment-frame buildings,” Soil Dynamics and

Earthquake Engineering, vol. 152, p. 107013, 2022.

[14] M. V. Requena-Garcia-Cruz et al., "Seismic SSI effects on the vulnerability of RC buildings," Engineering Structures, vol. 254, p. 113849, 2022.

[15] A. S. Veletsos and J. W. Meek, "Dynamic behaviour of building-foundation systems," Earthquake Engineering & Structural Dynamics, vol. 3, no. 2, pp. 121–138, 1974.

[16] K. A. Wani, R. Showkat, and S. A. Lone, "Evaluation of SSI effects on the dynamic response of high-rise buildings with mat foundations," IJARSCT, vol. 2, no. 1, pp. 226–237, 2022.

[17] J. Young, M. C. Griffith, and N. T. K. Lam, "Seismic response of high-rise frame buildings to far-field ground motions considering SSI," Bulletin of Earthquake Engineering, vol. 22, no. 3, pp. 1345–1372, 2024.

[18] L. Zhang and H. Far, "Seismic performance of high-rise buildings considering SSI with different foundation types," Structures, vol. 58, p. 105432, 2024.

[19] Pacific Earthquake Engineering Research Center (PEER), PEER NGA-West2 Ground Motion Database. Berkeley, CA, USA: Univ. California, Berkeley, 2014. [Online]. Available: https://ngawest2.berkeley.edu